

MALDI mass spectrometry imaging analysis of pituitary adenomas for near-real-time tumor delineation

David Calligaris^{a,1}, Daniel R. Feldman^{a,1}, Isaiah Norton^a, Olutayo Olubiyi^a, Armen N. Changelian^a, Revaz Machaidze^{a,b}, Matthew L. Vestal^a, Edward R. Laws^a, Ian F. Dunn^a, Sandro Santagata^{b,c}, and Nathalie Y. R. Agar^{a,c,d,2}

^aDepartment of Neurosurgery, Brigham and Women's Hospital, Harvard Medical School, Boston, MA 02115; ^bDepartment of Pathology, Brigham and Women's Hospital, Harvard Medical School, Boston, MA 02115; ^cDepartment of Cancer Biology, Dana-Farber Cancer Institute, Boston, MA 02115; and ^dDepartment of Radiology, Brigham and Women's Hospital, Harvard Medical School, Boston, MA 02115

Edited by Jerrold Meinwald, Cornell University, Ithaca, NY, and approved July 7, 2015 (received for review December 4, 2014)

We present a proof of concept study designed to support the clinical development of mass spectrometry imaging (MSI) for the detection of pituitary tumors during surgery. We analyzed by matrix-assisted laser desorption/ionization (MALDI) MSI six non-pathological (NP) human pituitary glands and 45 hormone secreting and nonsecreting (NS) human pituitary adenomas. We show that the distribution of pituitary hormones such as prolactin (PRL), growth hormone (GH), adrenocorticotrophic hormone (ACTH), and thyroid stimulating hormone (TSH) in both normal and tumor tissues can be assessed by using this approach. The presence of most of the pituitary hormones was confirmed by using MS/MS and pseudo-MS/MS methods, and subtyping of pituitary adenomas was performed by using principal component analysis (PCA) and support vector machine (SVM). Our proof of concept study demonstrates that MALDI MSI could be used to directly detect excessive hormonal production from functional pituitary adenomas and generally classify pituitary adenomas by using statistical and machine learning analyses. The tissue characterization can be completed in fewer than 30 min and could therefore be applied for the near-real-time detection and delineation of pituitary tumors for intraoperative surgical decision-making.

mass spectrometry imaging | pituitary | molecular pathology | intrasurgical diagnosis | in-source decay

Pituitary adenomas are common, benign intracranial tumors arising in the anterior pituitary gland (1–3) and are the third most common primary brain tumor. These tumors are classified according to both their size—microadenomas have a diameter less than 1 cm, whereas macroadenomas have a diameter equal to or larger than 1 cm—and by their functional status. Some tumors produce supraphysiologic quantities of hormones normally secreted by the pituitary gland and are referred to as functional adenomas, whereas others do not and are termed nonfunctioning tumors. The mass effect resulting from large adenomas that have parasellar or suprasellar extension can produce headaches, diplopia, visual field defects, cranial nerve palsies, and pituitary dysfunction due to compression of the pituitary gland and surrounding brain structures (4). Hormone-secreting adenomas [for instance, those that produce excess prolactin (PRL), growth hormone (GH), adrenocorticotrophic hormone (ACTH), or thyroid stimulating hormone (TSH)] can generate a broad range of endocrine disturbances and comorbidities related to the specific hormone being secreted in excess (5–9).

Transsphenoidal surgical approaches are the most common first-line treatment for pituitary adenomas that require surgical intervention. These procedures relieve the compression of critical structures by macroadenomas, and reduce or eliminate abnormal hormonal hypersecretion by hormone-producing adenomas (10–12). Microadenomas can be radiologically difficult or impossible to detect because of their smaller volume, but clinical presentations such as overproduction of hormones (e.g., ACTH, inducing Cushing syndrome) warrant surgical intervention. In such cases where MRI scans are equivocal, surgical planning is

based on inferior petrosal sinus sampling that may help determine the side of the pituitary involved and direct the extent of surgery. Determining the extent of tumor resection even when preoperative radiologic images are available for surgical guidance can be difficult, and incomplete resection and residual tumor may result. In macroadenomas, intraoperative magnetic resonance imaging (MRI) can be used to evaluate the extent of resection (13), but access to such a resource can be limited. Fluorescence approaches can also be used to evaluate the extent of resection: Using indocyanine green (ICG) fluorescence during endoscopic endonasal transsphenoidal surgery can help differentiate adenoma from normal pituitary tissue by detecting the near-infrared light that is emitted by ICG from the microvasculature of the normal pituitary and the adjacent tumor tissue (14). The reliable discrimination of pituitary tumor from normal pituitary gland remains a central issue in the successful surgical resection of these tumors given the desire to preserve or even restore normal pituitary function in patients.

Determination of serum hormone levels is an important part of the clinical evaluation of patients with pituitary adenomas. Imaging tests such as MRI and computed tomography (CT) are also used, but the resolution of such imaging technologies is limited to a scale of millimeters, so these studies may not detect very small microadenomas. The normal pituitary is composed of an anterior lobe (adenohypophysis) and a posterior lobe (neurohypophysis) with zonal distributions of various secretory cells. The adenohypophysis contains GH-producing cells located in

Significance

This study presents the use of matrix-assisted laser desorption/ionization (MALDI) mass spectrometry imaging (MSI) to detect and delineate pituitary tumors. Using MALDI MSI, it is possible to determine the peptide and protein hormone composition of pituitary tumor resection samples in fewer than 30 min. Surgeons could therefore have access to critical information for surgical decision-making in a near-real-time manner and be able to localize and discriminate pituitary tumor from non-pathological pituitary gland. This study supports the inclusion of MALDI MSI in the clinical workflow for the surgical resection of pituitary tumors, potentially allowing for improved surgical precision and patient outcomes.

Author contributions: D.C., E.R.L., and N.Y.R.A. designed research; D.C., D.R.F., and A.N.C. performed research; E.R.L. and I.F.D. contributed new reagents/analytic tools; D.C., D.R.F., I.N., O.O., R.M., M.L.V., and S.S. analyzed data; D.C. and N.Y.R.A. wrote the paper; and E.R.L. and I.F.D. provided the samples.

Conflict of interest statement: In compliance with Harvard Medical School and Partners Healthcare guidelines on potential conflict of interest, we disclose that S.S. and N.Y.R.A. are scientific advisors to BayesianDx.

This article is a PNAS Direct Submission.

¹D.C. and D.R.F. contributed equally to this work.

²To whom correspondence should be addressed. Email: nathalie_agar@dfci.harvard.edu.

This article contains supporting information online at www.pnas.org/lookup/suppl/doi:10.1073/pnas.1423101112/-DCSupplemental.

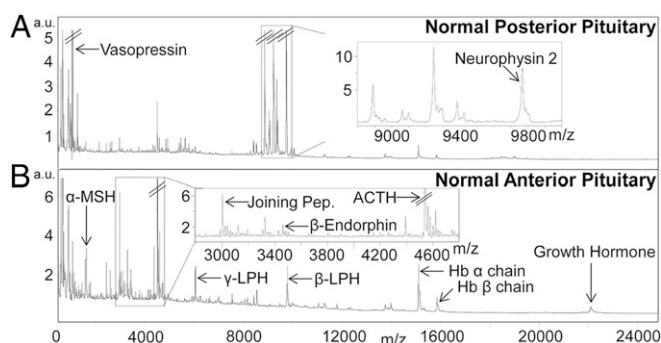


Fig. 1. Average MALDI mass spectra of a NP human pituitary gland (NP2). Average MALDI mass spectra of the anterior (A) and posterior (B) lobes of a NP pituitary section.

the lateral wings, PRL-producing cells in the posterior lateral areas, TSH-producing cells in the anterior midline area, follicle stimulating hormone (FSH) or luteinizing hormone (LH)-producing cells throughout the adenohypophysis, and ACTH-producing cells in the midline area extending back into the neurohypophysis. The neurohypophysis comprises axons from neurons that originate in the hypothalamus and that secrete oxytocin and vasopressin (15). The ACTH-related pituitary hormones are processing products of a common precursor protein named pro-opiomelanocortin (POMC). Enzymatic cleavage of this prohormone produces the following peptides: signal peptide, N-terminal glycopeptide, γ -melanocyte-stimulating hormone (γ -MSH), joining peptide, ACTH, α -melanocyte-stimulating hormone (α -MSH), corticotropin-like intermediate peptide (CLIP), β -lipotropin (β -LPH), γ -lipotropin (γ -LPH), and β -endorphin (16).

The development of new intraoperative techniques to analyze the distribution of specific pituitary hormones could be helpful for surgeons as they strive to better define the location and the boundaries of the pituitary adenomas, thereby improving the extent of resection and minimizing damage to normal pituitary structures. Mass spectrometry imaging (MSI) has been recognized as a powerful tool for the molecular profiling and imaging of a variety of tumors. This technique has been used for characterizing molecules such as proteins, peptides, lipids, and metabolites in tissue samples (17–24). Desorption electrospray ionization (DESI) coupled with MSI has already been shown to distinguish cancerous from noncancerous tissue, and studies validating its implementation in an operating room for real-time and near-real-time diagnosis have been presented (25–28). Matrix assisted laser desorption/ionization mass spectrometry imaging (MALDI MSI) has also shown great promise in supporting approaches already used in clinical diagnostic practice (29–32).

Here, we present a proof of concept study for the analysis of pituitary adenomas by MALDI MSI for surgical application. First, we used MALDI MSI to characterize the distribution of specific hormones such as ACTH and GH in the adenohypophysis, and vasopressin and neurophysin 2 in the neurohypophysis of normal human pituitary glands. We further used MALDI MSI to characterize a series of pituitary adenomas, and confirmed the identity of these pituitary hormones by using a high-resolution sequencing approach (LIFT) and in-source decay (ISD) methods. Our study demonstrates that the hormone composition of pituitary tumor resection samples can be assessed by using MALDI MSI within the time constraints of surgical intervention. This top-down approach might support the localization of small tumors within the gland, the delineation of tumor margins in a near-real-time diagnostic platform, and aid in the improved discrimination of tumor, which is to be resected, from normal gland, which is to be preserved.

Results and Discussion

Analysis of a Nonpathological Human Pituitary. The peptides produced by the anterior and the posterior lobes of the pituitary carry specific physiological functions. They can be overexpressed in pituitary adenomas and could potentially be used as biomarkers in molecular image-guided surgery.

We assessed baseline levels and distribution of these peptides by imaging nonpathological (NP) human pituitary glands by MALDI MS in linear positive ion mode in the mass/charge (m/z) range of 500–30,000. Fig. 1 shows representative mass spectra from MALDI MSI analyses corresponding to the signal detected in the posterior and the anterior regions of a human pituitary gland (sample NP2, see *SI Appendix, Table S1* for details). The mass spectra displayed show distinct peaks from the posterior (Fig. 1A) and the anterior (Fig. 1B) regions of the pituitary gland, in accordance with known histology of the gland (19). According to the theoretical masses calculated from the amino acid sequences of the POMC prohormone cleavage products, these peaks can be assigned to vasopressin (m/z 1,084.4) and neurophysin 2 (m/z 9,768.1) in Fig. 1A and to α -MSH (m/z 1,623.7), joining peptide 105–134 (m/z 3,004.3), β -endorphin (m/z 3,463.7), ACTH (m/z 4,539.2), γ -LPH (m/z 6,071.4), β -LPH (m/z 9,800.9), and growth hormone (m/z 22,106.6) in Fig. 1B. Additional proteins were detected by using another matrix deposition approach based on matrix sublimation followed by recrystallization to optimize incorporation of the analytes into the deposited matrix (33).

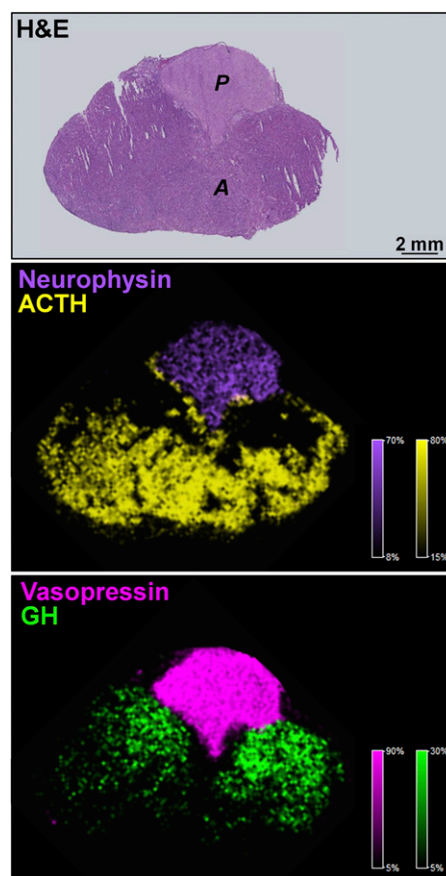


Fig. 2. MALDI MSI on a NP pituitary gland section (NP2). Top shows the optical image of a serial section H&E stained. Middle and Bottom display the MALDI MSI ion images of ACTH and neurophysin 2 and of vasopressin and GH, respectively. A and P indicate the anterior and posterior lobes of the pituitary gland, respectively.

Neurophysin 1 and PRL were also detected, respectively, in the posterior and the anterior lobes (*SI Appendix, Fig. S1*).

MALDI MSI images of Fig. 2 and *SI Appendix, Fig. S3* show the distribution of ACTH, neurophysin 2, vasopressin, growth hormone, and PRL for both sets of experiments (i.e., matrix deposition by spraying or by sublimation). The detection of PRL, GH, ACTH, and TSH has clinical significance because their excessive production by tumor may result in specific clinical syndromes with associated morbidity. Vasopressin detection may also have clinical significance; injury to vasopressin-secreting cells may result in diabetes insipidus in patients, making preservation of the posterior gland and stalk a goal of surgery. Both vasopressin and neurophysin 2 were detected from the posterior pituitary, and are known to be produced from the same precursor, namely the vasopressin-neurophysin 2-copeptin precursor (34). Neurophysin 2 binds vasopressin to form a heterotetrameric complex protecting it from proteolysis and promoting proper precursor cleavage (35). As shown in Fig. 2, these proteins are both located in the posterior pituitary. As indicated on the schema of *SI Appendix, Fig. S2*, the spatial distribution of pituitary hormones correlates with the established mapping of the different pituitary cell types. The detection and distribution of ACTH and GH in the anterior lobe, and neurophysin 2 in the posterior lobe, correlate with histological mapping of the NP human pituitary gland (Fig. 2). Using matrix sublimation/recrystallization, a supplementary peak was detected at an *m/z* value corresponding to the mass of PRL (i.e., *m/z* 22,897). MALDI MSI data indicated that this molecule is located in the anterior lobe, more precisely in the lactotroph cells area (*SI Appendix, Fig. S3*).

Top-Down Protein Identification. The identity of proteins was further confirmed by using MALDI in-source decay (ISD) fragmentation. ISD fragmentation occurs in the ion source of the MALDI mass spectrometer and can lead to the formation of *c*- and *z*-fragment

ions, but also *a*-, *b*-, *x*-, and *y*-fragment ions depending on the MALDI matrix used (35–45). This approach has already been used for peptide and protein identification either in solution (38, 46, 47) or in situ (48–51).

SI Appendix, Fig. S4 shows a MALDI ISD MSI experiment performed on a NP human pituitary tissue section. The distribution of representative *c*-series ion fragments of ACTH (*c*₁₀), GH (*c*₁₃), and neurophysin 2 (*c*₁₆) correlates with the specific histologic features displayed on the hematoxylin and eosin (H&E)-stained section (i.e., anterior and posterior lobes), and the established map of the pituitary (*SI Appendix, Fig. S2*). All of the *c*-series ISD fragments belonging to each hormone triggered the same specific MALDI MSI signals. The Mascot search results for mass spectra selected from a pixel with maximum intensity from the MALDI ISD MSI data confirmed the identification of ACTH, GH, and neurophysin 2, with respective significance scores of 306, 132, and 955 (*SI Appendix, Figs. S5–S8*). ACTH was identified through identification of the POMC prohormone with sequence coverage of 14% (*SI Appendix, Fig. S8A*) corresponding exclusively to the complete amino acid sequence of ACTH. A peptide fragment of 43 amino acids (i.e., somatotropin 1–43) was identified as somatotropin 1–43 (*SI Appendix, Fig. S8B*), which results from a proteolytic cleavage of GH and has insulin-potentiating properties (52).

The identification of vasopressin in the NP pituitary gland was confirmed by using MALDI TOF/TOF through the detection of *b*- and *y*-series ions (*SI Appendix, Fig. S9*), but we could not confirm the identity of PRL by fragmentation patterns (53, 54). Prolactin was assigned based on its mass and characteristic spatial distribution.

Despite the fact that MALDI ISD has great advantages compared with conventional MS fragmentation approaches (i.e., collision-induced dissociation and postsorce decay), this technique presents several limitations. MALDI ISD occurs in the ion source and, therefore, precursor ions cannot be selected. Thus,

Table 1. Summary of mass spectrometry and histopathology results for all analyzed pituitary adenomas

Sample ID	Type of secreting adenoma*	MS analysis				Reticulin stain	Sample ID	Type of secreting adenoma*	MS analysis				Reticulin stain
		ACTH	GH	PRL					ACTH	GH	PRL		
A1	ACTH	+	—	—	Tumor	H8	GH and PRL	—	—	—	Tumor		
A2	ACTH	+	—	—	Tumor	H9	GH and PRL	+	+	+	Tumor		
A3	ACTH	+	+	—	Normal	O1	FSH and LH	—	—	—	Tumor		
A4	ACTH	+	—	—	Tumor	O2	FSH and LH	—	—	—	Tumor		
A5	ACTH	+	+	+	Normal	O4	FSH and LH	—	—	—	Tumor		
A6	ACTH	+	—	—	Tumor	O10	FSH and LH	—	—	—	Tumor		
H1	GH	—	+	—	Tumor	O12	FSH and LH	—	—	—	Tumor		
H2	GH	+	+	—	Tumor	N1	None	—	—	—	Tumor		
H3	GH	—	+	—	Tumor	N2	None	—	—	—	Tumor		
H4	GH	—	+	—	Tumor	N3	None	—	—	—	Tumor		
H6	GH	—	+	—	Tumor	N4	None	—	—	—	Tumor		
H10	GH	—	+	—	Tumor	N5	None	—	—	—	Tumor		
H11	GH	—	+	—	Tumor	N6	None	—	—	—	Tumor		
O3	PRL	+	+	—	Normal	N7	None	—	—	—	Tumor		
O5	PRL	—	—	—	Necrosis	N8	None	—	—	—	Tumor		
O6	PRL	—	—	—	Tumor	N9	None	—	—	—	Tumor		
O8	PRL	—	—	+	Tumor	N10	None	—	—	—	Tumor		
O9	PRL	—	—	+	Tumor	N11	None	—	—	—	Tumor		
O13	PRL	—	—	+	Tumor	N12	None	—	—	—	Tumor		
O7	FSH	—	—	—	Tumor	N13	None	—	—	—	Tumor		
O11	FSH	—	—	—	Tumor	N14	None	+	—	—	Tumor		
H5	GH and PRL	—	+	—	Tumor	N15	None	—	—	—	Tumor		
H7	GH and PRL	—	—	—	Tumor	—	—	—	—	—	—		

Each pituitary tumor was originally diagnosed based on the clinical findings. MALDI MSI was then conducted to attempt to confirm these same results. ACTH, adrenocorticotropic hormone; FSH, follicle-stimulating hormone; GH, growth hormone; LH, luteinizing hormone; PRL, prolactin.

*The type of secreting adenoma has been defined by blood testing.

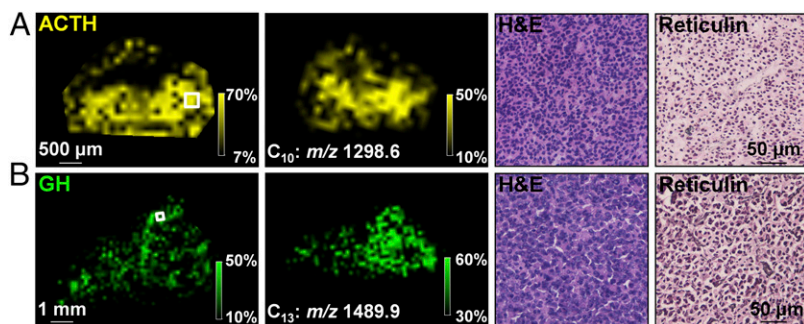


Fig. 3. Detection and confirmation of relevant proteins within functioning pituitary tumors by MALDI MSI and MALDI ISD MSI. (A) Ion images show the distribution of intact ACTH and one of its ISD fragments (C_{10} ion) within an ACTH secreting pituitary adenoma (sample A6). The H&E staining along with the absence of reticulin fiber rings from the reticulin stain indicate that this sample is a tumor. (B) Ion images show distribution of intact GH and an ISD fragment (C_{13} ion) within a GH secreting pituitary adenoma (sample H2). The H&E staining along with the absence of reticulin fiber compartments from the reticulin stain indicate that this sample is a tumor.

the analysis of complex samples such as tissue sections can lead to complicated mass spectra that impair the detection of ISD fragments from the proteins of interest. For low mass proteins, the presence of the matrix peaks in the low mass range can also prevent the observation of the ISD fragments. Other parameters can also be responsible for the nondetection of ISD fragments of vasopressin and PRL. Indeed, the formation of the fragment ions strongly depends on the nature of the amino acids present in the molecule (55), but also on the level of protein/peptide present in the sample (36, 37).

Molecular Characterization of Pituitary Adenomas. Using methodology developed for the analysis of the NP human pituitary, we analyzed 45 pituitary adenomas by MALDI MSI (Table 1) for the detection of ACTH, GH, and PRL. Elevated levels of these hormones in the most common functioning adenomas could be used for intraoperative detection and delineation of functioning tumors of the pituitary (1, 56) and, importantly, discrimination of tumor from the normal gland, which surgeons work to preserve. Most of the MS data were found to be identical to that of the original clinical findings, and results from this study are summarized in Table 1. Two representative examples are shown in Fig. 3. These samples were diagnosed as ACTH-secreting tumor (sample A6; Fig. 3A) and GH-secreting tumor (sample H2; Fig. 3B). From these samples, the relevant hormones and corresponding ISD fragments were detected by MALDI MSI and ISD MSI, respectively (Fig. 3). We confirmed the identification by Mascot searches from ISD mass spectra extracted from both MALDI ISD MSI analyses with significance scores of 697 (ACTH, sample A6) and 368 (GH, sample H2) (*SI Appendix*, Figs. S10–S12).

Using MALDI ISD MSI we also detected PRL from a series of adenoma samples diagnosed as prolactinomas. Imaging of PRL is shown in Fig. 4 for two different samples, namely O9 and O13. We did not detect the presence of PRL in one of the studied prolactinomas (sample O6), but further review of the H&E staining revealed a complex histology with calcification that could suppress the signal.

To resolve normal and pathological regions in pituitary tumor sections, we correlated results to the histopathological evaluation of both H&E and reticulin staining. The normal anterior pituitary gland typically consists of an intact reticulin fiber network formed around a small cluster of cells, whereas this fiber network is disrupted in tumors (57). A representative example of an intact reticulin network is shown in *SI Appendix*, Fig. S13. ACTH was detected and correlated to normal regions of tissue from tumor, and presumed to represent normal ACTH levels. Similarly, other hormones such as GH and PRL were detected from normal regions of the tumor samples and thought to be indicative of the anatomical presentation of the tumor (*SI Appendix*, Table S2). A nonfunctioning pituitary adenoma, sample N5, only showed three focal regions with ACTH and GH, which correlated with normal tissue regions according to reticulin staining (*SI Appendix*, Fig. S14).

Approach to Tumor Localization and Delineation. In addition to the ability to detect the relevant hormone biomarkers, some additional limiting criteria for application of the analyses for surgical application include time of execution and specificity. The execution of the presented protocol, which relies on the direct identification of protein/peptide hormones from tissue sections, requires less than 30 min, which falls within the timeline of pituitary surgery. A typical pituitary adenoma operation lasts

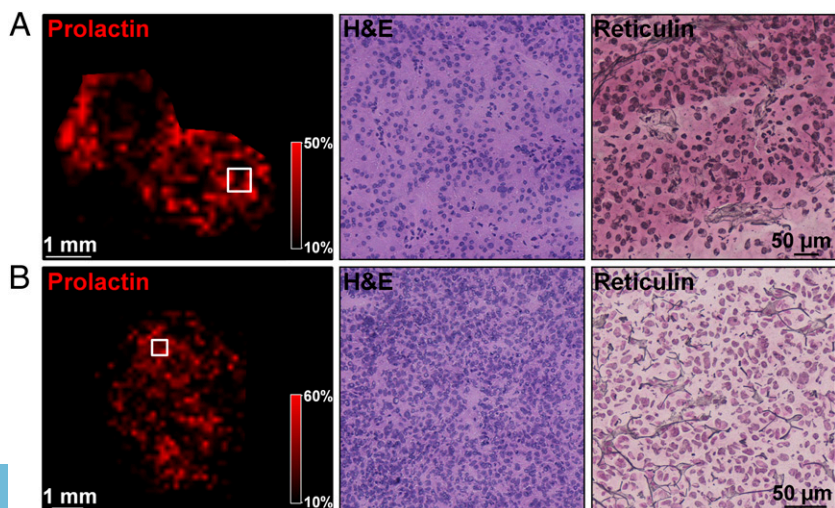


Fig. 4. MALDI MSI analysis of prolactin secreting pituitary adenomas O9 and O13. (A) Left shows a MALDI MSI ion image displaying the distribution of prolactin (m/z 22,884.6) in sample O9. Middle and Right display the optical images of serial sections, H&E stained (Middle) or stained for reticulin (Right). The reticulin staining indicates that this sample is a pituitary adenoma. (B) Left shows a MALDI MSI ion image displaying the distribution of prolactin (m/z 22,884.9) in sample O13. Middle and Right display the optical images of serial sections, H&E stained (Middle) or stained for reticulin (Right). The reticulin staining indicates that this sample is also a pituitary adenoma.

90 min to 3 h, allowing ample time for MALDI MS analysis. The value brought from the ability to (i) detect the tumor and (ii) delineate it from NP pituitary outweighs the current time limitation of the method. The specificity in detecting pituitary adenomas is further challenged by the fact that the adenomas, and more specifically the secreting adenomas, produce hormones that are also produced by the normal pituitary tissue, but at a higher level. One approach would be to quantitate levels and establish a threshold to be considered abnormal. A second approach, which we have applied, is to increase the specificity of tumor delineation by using the additional information found in the mass spectra. To do so, we performed principal component analysis (PCA) to highlight the different protein signatures existing between the NP pituitary glands and the nonsecreting (NS)/secreting pituitary adenoma samples. The first PCA was performed on data from four ACTH secreting adenoma and six NP human pituitary glands (Fig. 5A). The first three principal components (PCs) of the pituitary samples protein profiling data show two specific groupings corresponding to the mass spectra acquired on the ACTH secreting adenomas samples (red dots; Fig. 5A) and the NP human pituitary gland samples (green dots; Fig. 5A). The same results are observed between the mass spectra acquired from five GH (red dots; Fig. 5B), four GH PRL (green dots; Fig. 6B), or five FSH LH (red dots; Fig. 5C) secreting adenoma samples and six NP human pituitary gland samples (blue dots; Fig. 5B and C). Sensitivity and specificity of MALDI MSI data for distinguishing secreting pituitary adenomas from normal pituitary based on specific hormones were evaluated and results are presented in *SI Appendix, Table S3*. Using preoperative laboratory diagnosis of the secreting pituitary adenomas and histopathology evaluation of the tissue as gold standards (i.e., blood tests results and reticulin staining of Table 1), we estimated the overall sensitivity and specificity of the MALDI MSI data in identifying ACTH, GH, and PRL secreting pituitary adenomas from NP pituitary to be 83% and 93%, respectively (*SI Appendix, Table S3*).

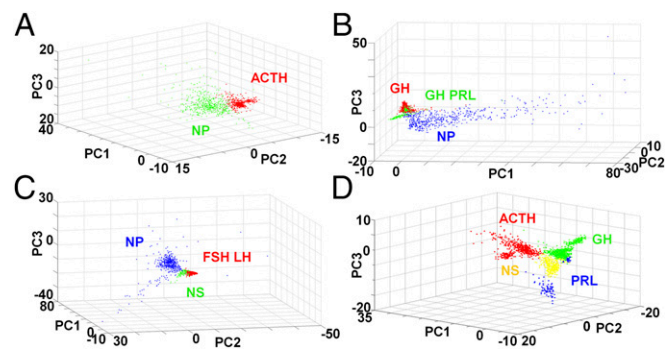


Fig. 5. PCA of MALDI MSI data from NP human pituitary glands, and secreting and nonsecreting pituitary adenomas. (A) Score plot of the three first principal components (PC1–PC3) displaying mass spectra from four ACTH secreting pituitary adenomas (A1, A2, A4, and A6; ACTH red dots) and six NP human pituitary glands (NP green dots). (B) Score plot of the three first principal components (PC1–PC3) displaying mass spectra from five GH (H1, H2, H4, H6, and H10; GH red dots), four GH PRL (H5, H7, H8, and H9; GH PRL green dots) secreting pituitary adenomas, and six NP human pituitary glands (NP blue dots). (C) Score plot of the three first principal components (PC1–PC3) displaying mass spectra from five FSH LH secreting pituitary adenomas (O2, O4, O10, O11, and O12; FSH LH red dots), five NS pituitary adenomas (N6, N7, N8, N9, and N10; NS green dots), and six NP human pituitary glands (NP blue dots). (D) Score plot of the three first principal components (PC1–PC3) displaying mass spectra from four ACTH (A1, A2, A4, and A6; ACTH red dots), five GH (H1, H2, H4, H6 and H10; GH green dots), two prolactin (O9, O13; PRL blue dots) secreting pituitary adenomas, and five NS pituitary adenomas (N6, N7, N8, N9, and N10; NS yellow dots).

Table 2. Classification results for nonsecreting pituitary adenomas samples

Sample ID	Reticulin Stain	Tissue type, %	
		Normal	Nonsecreting
N2	Tumor	1	99
N6	Tumor	0	100
N7	Tumor	0	100
N9	Tumor	1	99
N10	Tumor	0	100
N13	Tumor	2	98
N15	Tumor	0	100
O3	Normal	98	2
NP5	Normal	100	0
NP6	Normal	100	0

Results indicate the percent of pixels within each region of interest selected for the analysis that were assigned to NS pituitary adenomas or NP pituitary class.

Nonsecreting adenomas can also be distinguished by PCA according to their protein signature from most but not all secreting adenomas. As shown in Fig. 5D, the PCA indicates that the mass spectra acquired from four ACTH (red dots; Fig. 5D), four GH (green dots; Fig. 5D), two PRL (blue dots; Fig. 5D) secreting adenoma samples, and five NS adenoma samples (yellow dots; Fig. 5D) cluster separately, whereas a substantial overlap exists among the mass spectra of the five FSH LH secreting (red dots; Fig. 5C) and the NS adenoma samples (green dots; Fig. 5C). A classification model using machine learning was further developed to discriminate nonsecreting pituitary adenomas from NP pituitary glands. The leave-one-out cross-validation and recognition capability of the classifier were, respectively, 99.83% and 100% in the training dataset. Classification results reported in Table 2 indicate that NS pituitary adenoma can be distinguished from NP pituitary gland by MALDI MSI. PCA and probabilistic latent semantic analysis (pLSA) results highlight the delineation between the two groups and the differentiating molecular species (*SI Appendix, Figs. S15 and S16*).

Conclusion

MALDI MSI provides the ability to directly detect excess hormonal production in functional adenomas and to subtype pituitary adenomas according to their broader protein signatures. The top-down approach was developed and validated by using NP human pituitary glands for which it resolved the hormonal topography of the NP pituitary gland, consistent with the current understanding of the geographic distribution of protein-producing cells. The methodology can be performed under 30 min so it may aid in the localization and delineation of adenomas; the discrimination of tumor from normal gland; and in the preservation of the posterior gland cells secreting vasopressin. The ability to rapidly characterize pituitary tissue at the molecular level may facilitate surgical resection and anterior and posterior gland preservation to optimize patient outcomes.

Materials and Methods

The 6 human nonpathological pituitary glands and 45 pituitary adenoma samples were prepared for histological and MALDI MS analyses. All of the protocols including tissue preparation, matrix deposition, MS analyses, and histochemistry are detailed in *SI Appendix, SI Materials and Methods*. The methods used for protein identification using ISD data and Mascot searches, and for statistical analyses using SVM analysis, sensitivity, and specificity estimation of the MALDI MSI data in identifying secreting pituitary adenomas from NP pituitary, PCA, and pLSA are also described.

ACKNOWLEDGMENTS. This work was funded in part by National Institute of Health (NIH) Director's New Innovator Award 1DP2OD007383-01 (to N.Y.R.A.); US

Army Medical Research/Center for Integration of Medicine and Innovative Technology (CIMIT) Grant 2010A052245; the National Center for Image Guided Therapy Grant P41RR019703; NIH Grant K08NS064168 (to S.S.); Pediatric Low Grade

Astrocytoma Program at Dana-Farber Cancer Institute; the Brain Science Foundation; and the Daniel E. Ponton fund for the Neurosciences at Brigham and Women's Hospital (BWH).

- Ezzat S, et al. (2004) The prevalence of pituitary adenomas: A systematic review. *Cancer* 101(3):613–619.
- Ezzat S, Asa SL (2006) Mechanisms of disease: The pathogenesis of pituitary tumors. *Nat Clin Pract Endocrinol Metab* 2(4):220–230.
- Fernandez A, Karavitaki N, Wass JA (2010) Prevalence of pituitary adenomas: A community-based, cross-sectional study in Banbury (Oxfordshire, UK). *Clin Endocrinol (Oxf)* 72(3):377–382.
- Pisaneschi M, Kapoor G (2005) Imaging the sella and parasellar region. *Neuroimaging Clin N Am* 15(1):203–219.
- Elamin MB, et al. (2008) Accuracy of diagnostic tests for Cushing's syndrome: A systematic review and meta-analysis. *J Clin Endocrinol Metab* 93(5):1553–1562.
- Melmed S, et al.; Endocrine Society (2011) Diagnosis and treatment of hyperprolactinemia: An Endocrine Society clinical practice guideline. *J Clin Endocrinol Metab* 96(2):273–288.
- Nieman LK, et al. (2008) The diagnosis of Cushing's syndrome: An Endocrine Society Clinical Practice Guideline. *J Clin Endocrinol Metab* 93(5):1526–1540.
- Freda PU, et al.; Endocrine Society (2011) Pituitary incidentaloma: An endocrine society clinical practice guideline. *J Clin Endocrinol Metab* 96(4):894–904.
- Arafah BM, Prunty D, Ybarra J, Hlavin ML, Selman WR (2000) The dominant role of increased intrasellar pressure in the pathogenesis of hypopituitarism, hyperprolactinemia, and headaches in patients with pituitary adenomas. *J Clin Endocrinol Metab* 85(5):1789–1793.
- Locatelli M, et al. (2013) The trans-sphenoidal resection of pituitary adenomas in elderly patients and surgical risk. *Pituitary* 16(2):146–151.
- Hardy J (1962) [Excision of pituitary adenomas by trans-sphenoidal approach]. *Union Med Can* 91:933–945.
- Komotar RJ, Starke RM, Raper DM, Anand VK, Schwartz TH (2012) Endoscopic endonasal compared with microscopic transsphenoidal and open transcranial resection of giant pituitary adenomas. *Pituitary* 15(2):150–159.
- Berkmann S, et al. (2011) Intraoperative magnetic resonance imaging and early prognosis for vision after transsphenoidal surgery for sellar lesions. *J Neurosurg* 115(3):518–527.
- Litvack ZN, Zada G, Laws ER, Jr (2012) Indocyanine green fluorescence endoscopy for visual differentiation of pituitary tumor from surrounding structures. *J Neurosurg* 116(5):935–941.
- Scheithauer B, Horvath E, Lloyd R, Kovacs K (2001) Pathology of Pituitary Adenomas and Pituitary Hyperplasia. *Diagnosis and Management of Pituitary Tumors*, eds Thapar K, Kovacs K, Scheithauer B, Lloyd R (Humana, New York), pp 91–154.
- Bicknell AB (2008) The tissue-specific processing of pro-opiomelanocortin. *J Neuroendocrinol* 20(6):692–699.
- Thomas A, et al. (2013) Histology-driven data mining of lipid signatures from multiple imaging mass spectrometry analyses: Application to human colorectal cancer liver metastasis biopsies. *Anal Chem* 85(5):2860–2866.
- Cimino J, et al. (2013) Towards lipidomics of low-abundant species for exploring tumor heterogeneity guided by high-resolution mass spectrometry imaging. *Int J Mol Sci* 14(12):24560–24580.
- Caprioli RM, Farmer TB, Gile J (1997) Molecular imaging of biological samples: Localization of peptides and proteins using MALDI-TOF MS. *Anal Chem* 69(23):4751–4760.
- Wang HY, Wu HW, Tsai PJ, Liu CB (2012) MALDI-mass spectrometry imaging of desalted rat brain sections reveals ischemia-mediated changes of lipids. *Anal Bioanal Chem* 404(1):113–124.
- Balluff B, et al. (2011) MALDI imaging identifies prognostic seven-protein signature of novel tissue markers in intestinal-type gastric cancer. *Am J Pathol* 179(6):2720–2729.
- Elsner M, et al. (2012) MALDI imaging mass spectrometry reveals COX7A2, TAGLN2 and S100-A10 as novel prognostic markers in Barrett's adenocarcinoma. *J Proteomics* 75(15):4693–4704.
- Grobe N, Elased KM, Cool DR, Morris M (2012) Mass spectrometry for the molecular imaging of angiotensin metabolism in kidney. *Am J Physiol Endocrinol Metab* 302(8):E1016–E1024.
- Cerruti CD, Benabdellah F, Laprévotte O, Touboul D, Brunelle A (2012) MALDI imaging and structural analysis of rat brain lipid negative ions with 9-aminoacridine matrix. *Anal Chem* 84(5):2164–2171.
- Calligaris D, et al. (2014) Application of desorption electrospray ionization mass spectrometry imaging in breast cancer margin analysis. *Proc Natl Acad Sci USA* 111(42):15184–15189.
- Santagata S, et al. (2014) Intraoperative mass spectrometry mapping of an oncometabolite to guide brain tumor surgery. *Proc Natl Acad Sci USA* 111(30):11121–11126.
- Eberlin LS, et al. (2013) Ambient mass spectrometry for the intraoperative molecular diagnosis of human brain tumors. *Proc Natl Acad Sci USA* 110(5):1611–1616.
- Calligaris D, et al. (2013) Mass spectrometry imaging as a tool for surgical decision-making. *J Mass Spectrom* 48(11):1178–1187.
- Schöne C, Höfler H, Walch A (2013) MALDI imaging mass spectrometry in cancer research: Combining proteomic profiling and histological evaluation. *Clin Biochem* 46(6):539–545.
- Bateson H, Saleem S, Loadman PM, Sutton CW (2011) Use of matrix-assisted laser desorption/ionisation mass spectrometry in cancer research. *J Pharmacol Toxicol Methods* 64(3):197–206.
- McDonnell LA, Heeren RM, Andrén PE, Stoeckli M, Corthals GL (2012) Going forward: Increasing the accessibility of imaging mass spectrometry. *J Proteomics* 75(16):5113–5121.
- Dihazi H, et al. (2013) Mass spectrometry imaging: Linking molecule profiles to tissue spatial distribution. *Expert Rev Proteomics* 10(1):17–20.
- Yang J, Caprioli RM (2011) Matrix sublimation/recrystallization for imaging proteins by mass spectrometry at high spatial resolution. *Anal Chem* 83(14):5728–5734.
- Mohr E, Hillers M, Ivell R, Haulica ID, Richter D (1985) Expression of the vasopressin and oxytocin genes in human hypothalamus. *FEBS Lett* 193(1):12–16.
- Kaźmierkiewicz R, Czaplowski C, Ciarkowski J (1997) Elucidation of neurophysin/bioligand interactions from molecular modeling. *Acta Biochim Pol* 44(3):453–466.
- Suckau D, Resemann A (2003) T3-sequencing: Targeted characterization of the N- and C-termini of undigested proteins by mass spectrometry. *Anal Chem* 75(21):5817–5824.
- Suckau D, Resemann A (2009) MALDI Top-Down sequencing: Calling N- and C-terminal protein sequences with high confidence and speed. *J Biomol Tech* 20(5):258–262.
- Calligaris D, et al. (2010) MALDI in-source decay of high mass protein isoforms: Application to alpha- and beta-tubulin variants. *Anal Chem* 82(14):6176–6184.
- Menger RF, et al. (2012) MALDI mass spectrometric imaging of cardiac tissue following myocardial infarction in a rat coronary artery ligation model. *Anal Chem* 84(2):1117–1125.
- Reiber DC, Brown RS, Weinberger S, Kenny J, Bailey J (1998) Unknown peptide sequencing using matrix-assisted laser desorption/ionization and in-source decay. *Anal Chem* 70(6):1214–1222.
- Asakawa D, Takayama M (2011) Specific cleavage at peptide backbone C α -C and CO-N bonds during matrix-assisted laser desorption/ionization in-source decay mass spectrometry with 5-nitrosalicylic acid as the matrix. *Rapid Commun Mass Spectrom* 25(17):2379–2383.
- Smargiasso N, Quinton L, De Pauw E (2012) 2-Aminobenzamide and 2-aminobenzoic acid as new MALDI matrices inducing radical mediated in-source decay of peptides and proteins. *J Am Soc Mass Spectrom* 23(3):469–474.
- Asakawa D, Takayama M (2011) C α -C bond cleavage of the peptide backbone in MALDI in-source decay using salicylic acid derivative matrices. *J Am Soc Mass Spectrom* 22(7):1224–1233.
- Demeure K, Quinton L, Gabelica V, De Pauw E (2007) Rational selection of the optimum MALDI matrix for top-down proteomics by in-source decay. *Anal Chem* 79(22):8678–8685.
- Sakakura M, Takayama M (2010) In-source decay and fragmentation characteristics of peptides using 5-aminosalicylic acid as a matrix in matrix-assisted laser desorption/ionization mass spectrometry. *J Am Soc Mass Spectrom* 21(6):979–988.
- Sellami L, et al. (2012) In-source decay and pseudo tandem mass spectrometry fragmentation processes of entire high mass proteins on a hybrid vacuum matrix-assisted laser desorption ionization-quadrupole ion-trap time-of-flight mass spectrometer. *Anal Chem* 84(12):5180–5185.
- Quinton L, et al. (2007) New method for characterizing highly disulfide-bridged peptides in complex mixtures: Application to toxin identification from crude venoms. *J Proteome Res* 6(8):3216–3223.
- Debois D, Bertrand V, Quinton L, De Pauw-Gillet MC, De Pauw E (2010) MALDI-in source decay applied to mass spectrometry imaging: A new tool for protein identification. *Anal Chem* 82(10):4036–4045.
- Ait-Belkacem R, et al. (2014) MALDI imaging and in-source decay for top-down characterization of glioblastoma. *Proteomics* 14(10):1290–1301.
- Calligaris D, et al. (2013) Selected protein monitoring in histological sections by targeted MALDI-FTICR in-source decay imaging. *Anal Chem* 85(4):2117–2126.
- Bonnel D, et al. (2011) Multivariate analyses for biomarkers hunting and validation through on-tissue bottom-up or in-source decay in MALDI-MSI: Application to prostate cancer. *Anal Bioanal Chem* 401(1):149–165.
- Lewis UJ, Sinha YN, Lewis GP (2000) Structure and properties of members of the hGH family: A review. *Endocr J* 47(Suppl):S1–S8.
- Suckau D, et al. (2003) A novel MALDI LIFT-TOF/TOF mass spectrometer for proteomics. *Anal Bioanal Chem* 376(7):952–965.
- Schnable V, et al. (2002) Screening for disulfide bonds in proteins by MALDI in-source decay and LIFT-TOF/MS. *Anal Chem* 74(19):4980–4988.
- Takayama M, Tsugita A (2000) Sequence information of peptides and proteins with in-source decay in matrix assisted laser desorption/ionization-time of flight-mass spectrometry. *Electrophoresis* 21(9):1670–1677.
- Osamura RY, et al. (2008) Pathology of the human pituitary adenomas. *Histochem Cell Biol* 130(3):495–507.
- Laws E, Ezzat S, Asa S, Rio L (2013) *Pituitary Disorders: Diagnosis and Management* (John Wiley & Sons, Malden, MA).